


Limit of Temporal Resolution in Atomic Force Microscopy: Speed of Imaging with Atomically Engineered Tips While Preserving Picometer-Range Spatial Resolution

Omur E. Dagdeviren*

Department of Physics, McGill University, Montréal, Québec, Canada H3A 2T8

 (Received 12 November 2018; revised manuscript received 23 December 2018; published 27 February 2019)

With recent advances in dynamic scanning probe microscopy techniques, it is now routine to image the submolecular structure of molecules with atomically engineered tips, which are prepared via controlled modification of the tip termination and are chemically well defined. The enhanced spatial resolution is possible as atomically engineered tips can preserve their integrity in the repulsive interaction regime. Although the mechanism of improved spatial resolution has been investigated both experimentally and theoretically, the ultimate temporal resolution while preserving picometer-scale spatial resolution still remains an open question. We computationally analyze the temporal resolution of atomic force microscopy imaging with atomically engineered tips. Our computational results reveal that nonmetal terminated tips, for example, oxygen-terminated copper, are well suited for enhanced temporal resolution up to video-rate imaging velocities while preserving picometer-range spatial resolution. On the other hand, the highest attainable spatial resolution of atomically engineered tips with low stiffness, for example, CO terminated, deteriorate with increasing imaging velocity. Our results reveal that when atomically engineered tips terminated with molecules are in use, imaging velocities of the order of nanometers per second at most are inevitable even for atomically flat surfaces to retain atomic resolution and avoid slip-stick motion. In addition to shedding light on the temporal resolution of atomic force microscopy imaging with atomically engineered tips, our numerical results provide an outlook to the scalability of atom-by-atom fabrication using scanning probe microscopy techniques.

DOI: [10.1103/PhysRevApplied.11.024068](https://doi.org/10.1103/PhysRevApplied.11.024068)

I. INTRODUCTION

Dynamic AFM is an analytical surface characterization tool where a sharp probe tip is mounted on the end of an oscillating probe and serves as a sensing element to disclose surface properties with picometer and piconewton resolution [1–3]. In recent years, imaging the submolecular structure of molecules has become popular with the advent of AFM and related techniques [4,5]. The termination of the tip apex is modified on purpose, that is, atomically engineered, either by picking up a molecule or a chemically identified atom [4–9]. One of the most widespread ways to engineer the tip apex is to pick a CO molecule, although other molecules can also be used [4,6,7]. Nonmetal terminated tips such as oxygen-, chlorine-, or bromine-terminated tips are alternatives to tips terminated with molecules [5,8,9]. Due to their inert nature, atomically engineered tips can preserve their integrity even in the repulsive tip-sample-interaction regime [4,5]. To understand a material's properties as a function of both their structural and chemical environments as well as its responses to external stimulations in ambient or liquid

environments, video-rate AFM has been developed but is currently limited to a lateral resolution of the order approximately equal to 10 nm [10–16]. In contrast, spatial characterization at atomic length scales is common practice under ultrahigh vacuum conditions; however, video-rate imaging is achieved only in scanning tunneling microscopy mode and thus is restricted to electronic properties [17]. We computationally explore the prospects of video-rate AFM imaging with atomically engineered tips while preserving picometer-range spatial resolution.

Our numerical results reveal that the temporal resolution depends on the tip-sample-interaction kinetics, which is dictated by the tip termination, tip-sample interaction force, and imaging velocity. The structural deformation of the tip apex, that is, the closest atom to the surface, upsurges with increasing imaging speeds and with decreasing stiffness of the tip apex. Our computational results disclose that nonmetal terminated tips such as oxygen-terminated copper tips, in principle, can display temporal resolution up to video-rate imaging velocities, while preserving picometer-range spatial resolution. However, tips with lower stiffness such as molecule-terminated tips are confined to slower imaging velocities that result in orders of magnitude longer image acquisition times. In addition

*omur.dagdeviren@mcgill.ca

to systematically examining the limits of temporal resolution in high-resolution AFM imaging with atomically engineered tips, our numerical analysis also provides an outlook of the scalability of atom-by-atom fabrication with dynamic scanning probe techniques and possible pathways for enhanced capability.

II. COMPUTATIONAL METHODS

Theoretical tools for high-resolution imaging with atomically engineered tips are well developed [5,18] (also see Ref. [19] by Jelínek for a review). Although more advanced kernels (see Refs. [5,18,19]) are available to model the tip-sample interaction of atomically engineered tips, we used Prandtl and Tomlinson (PT) to explain the interaction of a sharp probe tip with the surface [20–30]. The PT model has been successfully implemented to elucidate the interaction of an atomically sharp probe tip with flat surfaces, atomic steps, and alkali halide surfaces, and most recently to reveal the effect of surface disorder, load, and sliding velocity on friction at small length scales [21,26,31–34]. Most recently, Pawlak *et al.* (Ref. [7]) experimentally and theoretically demonstrated that the PT model can explain the tip-sample interaction of a single molecule attached to the end of an oscillating probe tip, which is modulated using noncontact AFM (also see Ref. [20] for a perspective). In this journal article, we apply the PT model to investigate the tip-sample interaction kinetics. As Fig. 1 summarizes, the change in the tip termination induces a change in the stiffness of the tip apex of an atomically engineered tip, which ultimately changes the tip-sample interaction kinetics and dictates the limits of spatial and temporal resolution of AFM imaging.

To disclose the tip-sample interaction kinetics of atomically engineered tips, the first step is to model the local tip-sample interaction. We use the 6–12 Lennard-Jones (LJ) interaction potential for our calculations [35]:

$$U_{LJ} = 4\epsilon[(\sigma/r)^{12} - (\sigma/r)^6]. \quad (1)$$

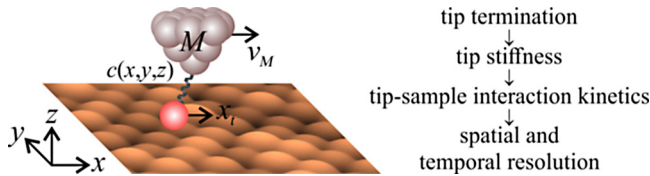


FIG. 1. The summary of computational methods. We use the two-dimensional PT model to investigate the kinetic interaction of the atomically sharp probe tip with the surface as a function of tip stiffness, normal load, and imaging velocity. The tip apex is connected to the microscope body, M , with an elastic spring constant of $c(x, y, z)$. The body of the microscope moves along the fast scan direction with the velocity v_M . The position of the tip apex (x_t, y_t, z_t) during the relative motion is determined by the tip-sample interaction kinetics.

In Eq. (1), U_{LJ} is the interaction potential of two atoms, r denotes the distance between the centers of the two atoms, ϵ is the depth of the potential well, and σ is the distance at which the potential well vanishes ($\sigma = d/1.12$, where d is the hard sphere diameter of the atom). We implement the periodic boundary conditions along the lateral directions to a simulation cell with a cross section of 33×33 atoms and a thickness of five atoms. The fast-scan direction is along the $\langle 110 \rangle$ direction of the simple cubic lattice [36]. We use typical parameters for metal atoms ($\epsilon = 415$ meV, $d = 2.6$ Å, Ref. [37]). The tip-sample interaction potential, U_{int} , is the summation of interaction potentials of all atoms within the simulation cell.

The next step is to model the probe tip. As Fig. 1 shows, the atomically sharp scanned probe is modeled as a single atom that is connected to the macroscopic body of the probe tip with an elastic spring (c_x, c_y, c_z spring constants along the x, y , and z directions). The stiffness of the spring changes with the termination of the atomically engineered tip and is different from the cantilevers used in scanning probe microscopy experiments [7,21,32,38].

We calculate the potential energy landscape in vacuum up to 6.5 Å with respect to the lattice position of the top layer with 2.5-pm steps for an area of 2.6×2.6 nm² in the center of the calculation slab. The distance between the tip and the sample is modulated to keep the force constant in most scanning probe microscopy experiments [2,3]. The vertical position of the tip can be expressed as:

$$\underbrace{c_z(z_M - z_{t,0})}_{F_z = \text{constant}} = \left. \frac{\partial U_{\text{int}}}{\partial z_t} \right|_{x_t, y_t}. \quad (2)$$

In Eq. (2), z_M is the position of the macroscopic body of the tip along the vertical direction. The stable position of the single-atom asperity along the z direction, $z_{t,0}$, for a fixed lateral coordinate (x_t, y_t) is calculated by equating the force acting on the spring-mass system along the vertical direction, F_z [the left-hand side of Eq. (2)], to the vertical component of the tip-sample interaction force for the fixed lateral coordinate (the right-hand side), which is calculated as the negative gradient of the total tip-sample interaction potential, U_{int} . The vertical height profile, the surface topography, is calculated for an area of 2.6×2.6 nm² in the center of the calculation slab. With the calculation of the equilibrium position of the apex atom along the z direction, the three-dimensional tip-sample interaction potential can be reduced to a two-dimensional interaction potential. The following two-dimensional system of coupled second-order differential equations is solved to calculate the motion of the atomically sharp tip along the lateral directions (x and y directions):

$$\begin{aligned} m_x \ddot{x}_t &= c_x(x_M - x_{t,0}) - \frac{\partial U(x_t, y_t)}{\partial x_t} - \gamma_x \dot{x}_t, \\ m_y \ddot{y}_t &= c_y(y_M - y_{t,0}) - \frac{\partial U(x_t, y_t)}{\partial y_t} - \gamma_y \dot{y}_t. \end{aligned} \quad (3)$$

Equation (3) is solved by using the ode45 function in MATLAB and restricting the relative error of the numerical solution to 10^{-10} [39]. In Eq. (3), m_x and m_y , 10^{-8} kg, are the effective masses of the system [26,31]. Coordinates of the tip-apex along the lateral directions are expressed as x_t and y_t , the time derivatives of the lateral positions' present velocity are (\dot{x}_t, \dot{y}_t) , and the acceleration of the atomically sharp probe tip is (\ddot{x}_t, \ddot{y}_t) . The total tip-sample interaction potential (U_{int}) is calculated numerically by adding up the contributions of all atoms in the simulation cell. We numerically calculate the negative gradient of the tip-sample interaction potential along the lateral directions, which produces the lateral force components of the interaction potential [40].

When the tip traces the surface, the kinetic energy [41] of the tip will be dissipated [28,42–44]. Different mechanisms, such as electronic [42,43,45–48], electromagnetic [49], van der Waals friction [50,51], and phononic [52–55], have been proposed for the energy dissipation due to kinetic tip-sample interaction. We include the effect of energy dissipation due to the motion of the tip with the damping coefficient term, γ , in Eq. (3). Figure 2 summarizes the numerical solution of Eq. (3) for the average slip length as a function of the damping coefficient. As Fig. 2 discloses, under the critical damping condition ($2\sqrt{c \times M}$, c and M are the spring constant and effective mass of the system), the average deformation is of the order of the unperturbed lattice constant (2.6 \AA) of the model system. Tip oscillations are evident for the underdamped case. For the strongly overdamped case, however, the tip sticks to a lattice site before slipping by multiple lattice constants, that is, the intrinsic contribution of the surface to the motion of the tip disappears. We use the critical damping coefficient in our calculations to eliminate tip oscillations and preserve contributions of the sample to the motion of the tip with our choice of damping coefficient. This choice of damping coefficient ensures that all slip events occur between adjacent unit cells, enables efficient computation, and is consistent with former experimental and theoretical studies [21,32].

Depending on the kinetic tip-sample interaction, the tip apex can either follow the minimum energy path or slip-stick motion may be evident, which impedes tracing the minimum energy trajectory and results in large structural deformations of the tip apex [33]. For this reason, the deformation length of the apex can be used as a caliber to quantify the kinetic tip-sample interaction between the tip and the sample. The total perturbation of the spring system from its equilibrium position, that is, the deformation length, is calculated by subtracting the position of the tip apex (x_t, y_t) from the unperturbed position of the macroscopic body of the microscope (x_M, y_M). This assumption is valid as long as the lateral stiffness of the cantilever probe is significantly larger than the stiffness of the tip apex. Experiments with atomically engineered tips

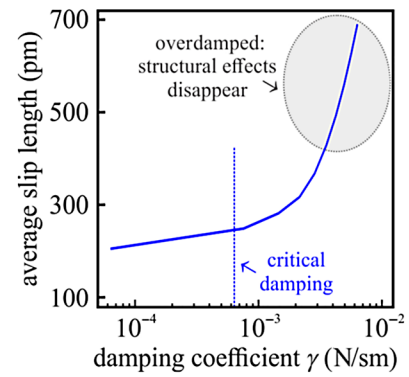


FIG. 2. The choice of damping coefficient, γ , to model the kinetic energy dissipation of the tip due to interaction with the surface. When the system is underdamped, strong tip oscillations are induced, while the contribution of the surface is diminished for the overdamped case. For these reasons, we use a critical damping condition to eliminate the tip oscillations while preserving the effect of the surface on the kinetic tip-sample interaction. We solve Eq. (3) for a model tip with a stiffness of 10 N/m and the effective mass, M , is equal to 10^{-8} kg for a normal load of 0.25 nN and a sliding velocity of 1000 nm/s for the calculations presented in Fig. 2.

are usually conducted with tuning forks in the qPlus configuration [4–7,56], which has a stiffness that ranges from a few kN/m to tens of kN/m [57,58]. For this reason, the contribution of the deflection of the cantilevers is neglected in our analysis. At the end of the scan frame, y_M is changed and a new line is calculated. To simulate the movement of the scanning force microscopy experiments, the tip starts with zero velocity at the left border of the scan area ($\dot{x}_t = 0, y_t = 0$) with relaxed springs ($x_M = 0, y_M = 0$). The transient part of the solution disappears within the first 5–6 \AA for the initial conditions defined for our calculations ($1 \text{ nm/s} \leq \dot{x}_M \leq 10\,000 \text{ nm/s}$). We exclude the transient part of the solution and use $2.0 \times 2.6 \text{ nm}^2$ at the center of the calculation slab for our statistical analyses. It has been shown that the mean value of the deformation length may not give statistically significant results [25]. To statistically evaluate the magnitude of the oscillating deflection, we use the rms deflection, which is the measure of the equivalent constant deflection over the calculation area.

III. RESULTS AND DISCUSSIONS

We analyze the interaction of the atomically sharp tip as a function of imaging velocity, the tip stiffness, and a normal load for an area of $2.0 \times 2.6 \text{ nm}^2$ at the center of the calculation slab. As Fig. 3 reveals, three distinct regions can be identified. In region I, the deformation length of the atomically sharp probe is less than 0.1 pm, which is significantly smaller than the highest spatial resolution that can be achieved with scanning probe techniques [40]. As highlighted in region I, the imaging velocity is less than a

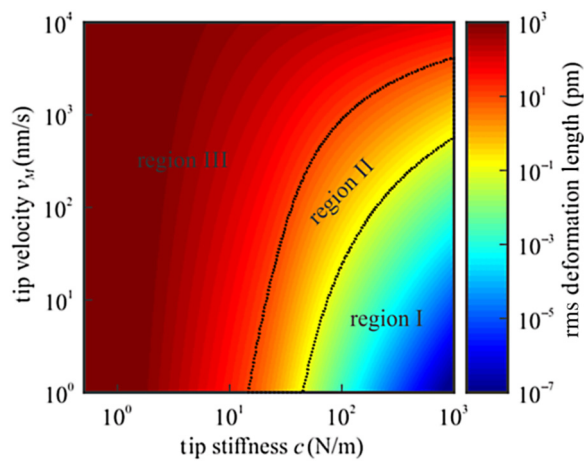


FIG. 3. The rms of the deformation length of an atomically sharp tip as a function of imaging velocity and tip stiffness. Three distinct regions are evident. The spatial resolution is restrained due to instrumental limitations in region I in which the deformation length is less than 0.1 pm. In region II, the stiffness of the atomically sharp tip is of the order of tens of nanonewtons and the picometer-range spatial resolution is preserved up to video-rate imaging velocities for nanometer size scans. The slip length limits the spatial resolution in region III, that is, slow imaging speeds are inevitable with the upsurge of the deformation length. The total vertical force acting on the tip is 200 piconewtons for the calculations presented in Fig. 3.

few hundred nanometers per second for atomically sharp tips with stiffness values that are of the order of hundreds of nanonewtons per meter. Although the atomically sharp probe tip sustains its integrity with subpicometer deformation in region I, the spatial resolution is constrained due to instrumental limitations such as readout noise and mechanical stability [59]. In region II, the spatial resolution is also preserved for high-resolution imaging. The deformation length of the tip apex is between 0.1 pm and 10.0 pm, which fits in the range of atomic-resolution images, and video-rate imaging velocities for atomic resolution images (1000 nm/s, roughly 400 lines per second) are attainable. On the contrary, in region III, the tip reveals deformations comparable to the lattice constant and the slip-stick motion is evident. The slip length also inflates with decreasing tip stiffness and slow imaging velocities of the order of subnanometers per second are inevitable to preserve the spatial resolution.

To elucidate the kinetic interaction of the atomically sharp probe tip and the surface, we investigate the deformation length as a function of normal load, tip stiffness, and the imaging velocity. As Fig. 4 reveals, we first explore the interaction of a tip with a 5-N/m stiffness, which is a comparable to atomically engineered tips with a porphyrin derivative molecule [7]. We conduct calculations for this relatively stiff molecule as softer molecules such

as CO lead to trivial results with significant deformations according to our calculations (Fig. 3). Experimental and computational results are available for an atomically engineered tip with a 5-N/m stiffness (Ref. [7]) to compare the findings of our model. As Figs. 4(a) and 4(b) show, the interaction of the atomically sharp tip displays slip-stick motion [for details, see inset in Fig. 4(a)]. It is worth noting that slip-stick motion is commonly observed for friction force microscopy studies [20–30]. Our results disclose that single-atom contacts can also reveal slip-stick motion, which is consistent with constant-height frequency modulation-based AFM experiments conducted with atomically engineered tips terminated with molecules at small oscillation amplitudes (less than 50 pm) [7]. In passing, it is important to mention that the nature of the tip, the tip-sample interaction length scale, and the oscillation amplitude may impede the use of the PT model to explain the AFM experiments. Also, as Fig. 4(c) shows, multiple slip-stick events are evident with increasing load for imaging speeds of the order of 1000 nm/s. In addition, we examine the kinetic tip-sample interaction of a tip with a stiffness of 50 N/m. This stiffness value approximates the springiness of an oxygen-terminated copper tip, which has two orders of magnitude larger stiffness [5,9] compared to CO-terminated copper tips (approximately 0.5 N/m, Refs. [19,60]). As highlighted by Figs. 4(d)–4(f), slip-stick events are not evident for the stiffer tip [for details, see inset in Fig. 4(d)]. Even though the deformation length increases with the load, the rms of the deformation length is of the order of 10 pm even for repulsive forces acting on the tip and the smooth tip motion is preserved with the absence of slip-stick motion.

Imaging velocities of the order of subnanometers per second are inevitable to achieve picometer spatial resolution “soft” atomically engineered tips, that is, tips terminated with a molecule. Otherwise, the spatial resolution attenuates due to slip-stick motion. As our numerical results demonstrate, with increasing imaging velocity, “stiffer” atomically engineered (e.g., oxygen-terminated copper) tips favor the preservation of the spatial resolution. As the slip-stick motion is eliminated with stiff atomically engineered tips, the atomically sharp tip can follow the lowest energy path [33]. For this reason, it is important to note that the tip deforms along both of the lateral directions. The deformation of the tip-apex along the slow-scan axis, that is, the direction perpendicular to v_M , may alter the interpretation of multidimensional force measurements or measured forces [61] and measured energy barriers of manipulation experiments [62].

In this work, we provide the ultimate theoretical limit for the imaging speed with atomically engineered tips. Our computational analysis does not take into account the additional noise sources and limitations of the measurement electronics, which may further scale down the maximum attainable imaging velocities. Also, the deformation of

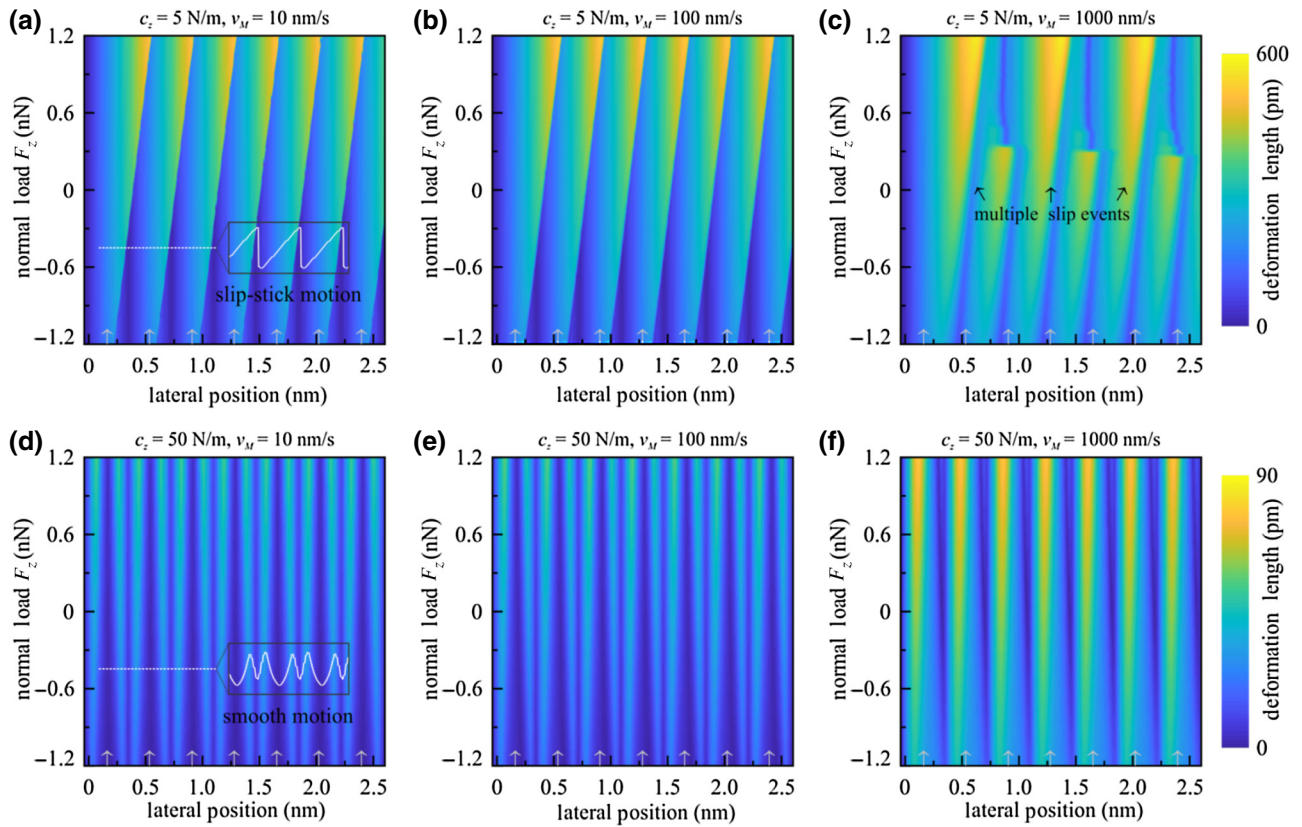


FIG. 4. Calculation of the deformation length as a function of tip stiffness, normal load, and imaging velocity for two different tip stiffnesses. (a)–(c) The stiffness values that are comparable to the stiffness of a molecule-terminated tip discloses slip-stick motion (e.g., profile of the dashed line in the inset in a), which is consistent with experimental results. With increasing stiffness (d)–(f), for example, an oxygen-terminated copper tip, the slip-stick motion is eliminated, for example, the profile of the dashed line in the inset in (d). White arrows show the center of surface atoms (a)–(f).

the surface or structures imaged (e.g., molecules) can constrain the imaging velocity. The effect of sample relaxations and the limitations induced by measurement electronics can be investigated in a further study using AFM simulation tools [63].

As an outlook, we want to mention that our results imply that the imaging chemical evolution of surfaces (i.e., chemical reactions) in real time with conventional AFM imaging have potential challenges with the available set of atomically engineered tips and due to instrumental constraints. Moreover, our results infer that scaling atom-by-atom fabrication with atomically engineered tips may have limitations if the atomic structure of the scanning probe is important.

IV. SUMMARY

We conduct numerical analysis to investigate the kinetics of tip-sample interaction of atomically engineered tips to reveal the limits of temporal resolution while preserving picometer-range spatial resolution by using the two-dimensional PT model. Our numerical results show

that the maximum temporal resolution of AFM imaging with atomically engineered tips is dictated by the stiffness of the tip apex. The structural deformation of the apex inflates with decreasing stiffness of the tip and increasing imaging speed and normal load. Our calculations show that “stiff” atomically engineered tips, such as oxygen-terminated copper tips, can withstand video-rate imaging velocities for atomic resolution images. On the contrary, tips with lower stiffness, for example, molecule-terminated tips, are confined to slower imaging velocities of the order of nanometers per second at most to preserve picometer-range spatial resolution. In addition, our results highlight that the scalability of atom-by-atom fabrication with dynamic probe techniques may face challenges if the atomic structure of the probe is important.

ACKNOWLEDGMENTS

I would like to thank Professor Peter Grütter, Dr. Yoichi Miyahara, and Mr. Harrisonn Griffin for fruitful discussions and critical reading of the manuscript. I also thank the referees for their comments, which further improved

the manuscript. Financial support from The Natural Sciences and Engineering Research Council of Canada and Le Fonds de Recherche du Québec - Nature et Technologies are gratefully acknowledged.

-
- [1] T. R. Albrecht, P. Grutter, D. Horne, and D. Rugar, Frequency modulation detection using high-Q cantilevers for enhanced force microscope sensitivity, *J. Appl. Phys.* **69**, 668 (1991).
- [2] R. Garcia, *Amplitude Modulation Atomic Force Microscopy* (Wiley-VCH, Singapore, 2010).
- [3] F. J. Giessibl, Advances in atomic force microscopy, *Rev. Mod. Phys.* **75**, 949 (2003).
- [4] L. Gross, F. Mohn, N. Moll, P. Liljeroth, and G. Meyer, The chemical structure of a molecule resolved by atomic force microscopy, *Science* **325**, 1110 (2009).
- [5] H. Mönig, D. R. Hermoso, O. Díaz Arado, M. Todorović, A. Timmer, S. Schüer, G. Langewisch, R. Pérez, and H. Fuchs, Submolecular imaging by noncontact atomic force microscopy with an oxygen atom rigidly connected to a metallic probe, *ACS Nano* **10**, 1201 (2016).
- [6] A. J. Weymouth, T. Hofmann, and F. J. Giessibl, Quantifying molecular stiffness and interaction with lateral force microscopy, *Science* **343**, 1120 (2014).
- [7] R. Pawlak, W. Ouyang, A. E. Filippov, L. Kalikhman-Razvovov, S. Kawai, T. Glatzel, E. Gnecco, A. Baratoff, Q. Zheng, O. Hod, M. Urbakh, and E. Meyer, Single-molecule tribology: Force microscopy manipulation of a porphyrin derivative on a copper surface, *ACS Nano* **10**, 713 (2016).
- [8] S. Kawai, A. S. Foster, T. Björkman, S. Nowakowska, J. Björk, F. F. Canova, L. H. Gade, T. A. Jung, and E. Meyer, Van der Waals interactions and the limits of isolated atom models at interfaces, *Nat. Commun.* **7**, 11559 (2016).
- [9] F. Mohn, B. Schuler, L. Gross, and G. Meyer, Different tips for high-resolution atomic force microscopy and scanning tunneling microscopy of single molecules, *Appl. Phys. Lett.* **102**, 073109 (2013).
- [10] T. Ando, N. Kodera, E. Takai, D. Maruyama, K. Saito, and A. Toda, A high-speed atomic force microscope for studying biological macromolecules, *Proc. Natl. Acad. Sci.* **98**, 12468 (2001).
- [11] T. Ando, T. Uchihashi, and T. Fukuma, High-speed atomic force microscopy for nano-visualization of dynamic biomolecular processes, *Prog. Surf. Sci.* **83**, 337 (2008).
- [12] P. K. Hansma, G. Schitter, G. E. Fantner, and C. Prater, High-speed atomic force microscopy, *Science* **314**, 601 (2006).
- [13] A. Toshio *et al.*, The 2018 correlative microscopy techniques roadmap, *J. Phys. D: Appl. Phys.* **51**, 443001 (2018).
- [14] T. Ando, High-speed atomic force microscopy and its future prospects, *Biophys. Rev.* **10**, 285 (2018).
- [15] A. P. Nievergelt, N. Banterle, S. H. Andany, P. Gönczy, and G. E. Fantner, High-speed photothermal off-resonance atomic force microscopy reveals assembly routes of centriolar scaffold protein SAS-6, *Nat. Nanotechnol.* **13**, 696 (2018).
- [16] J. D. Adams, B. W. Erickson, J. Grossenbacher, J. Brugger, A. Nievergelt, and G. E. Fantner, Harnessing the damping properties of materials for high-speed atomic force microscopy, *Nat. Nanotechnol.* **11**, 147 (2015).
- [17] F. Besenbacher, E. Lægsgaard, and I. Stensgaard, Fast-scanning STM studies, *Mater. Today* **8**, 26 (2005).
- [18] P. Hapala, G. Kichin, C. Wagner, F. S. Tautz, R. Temirov, and P. Jelínek, Mechanism of high-resolution STM/AFM imaging with functionalized tips, *Phys. Rev. B* **90**, 085421 (2014).
- [19] J. Pavel, High resolution SPM imaging of organic molecules with functionalized tips, *J. Phys.: Condens. Matter* **29**, 343002 (2017).
- [20] U. D. Schwarz and H. Hölscher, Exploring and explaining friction with the Prandtl–Tomlinson model, *ACS Nano* **10**, 38 (2016).
- [21] P. Steiner, R. Roth, E. Gnecco, A. Baratoff, and E. Meyer, Angular dependence of static and kinetic friction on alkali halide surfaces, *Phys. Rev. B* **82**, 205417 (2010).
- [22] C. M. Mate, G. M. McClelland, R. Erlandsson, and S. Chiang, Atomic-Scale Friction of a Tungsten Tip on a Graphite Surface, *Phys. Rev. Lett.* **59**, 1942 (1987).
- [23] E. Gnecco, R. Bennewitz, T. Gyalog, C. Loppacher, M. Bammerlin, E. Meyer, and H. J. Güntherodt, Velocity Dependence of Atomic Friction, *Phys. Rev. Lett.* **84**, 1172 (2000).
- [24] E. Riedo, E. Gnecco, R. Bennewitz, E. Meyer, and H. Brune, Interaction Potential and Hopping Dynamics Governing Sliding Friction, *Phys. Rev. Lett.* **91**, 084502 (2003).
- [25] L. Jansen, H. Hölscher, H. Fuchs, and A. Schirmeisen, Temperature Dependence of Atomic-Scale Stick-Slip Friction, *Phys. Rev. Lett.* **104**, 256101 (2010).
- [26] H. Hölscher, D. Ebeling, and U. D. Schwarz, Friction at Atomic-Scale Surface Steps: Experiment and Theory, *Phys. Rev. Lett.* **101**, 246105 (2008).
- [27] D. Gangloff, A. Bylinskii, I. Counts, W. Jhe, and V. Vuletić, Velocity tuning of friction with two trapped atoms, *Nat. Phys.* **11**, 915 (2015).
- [28] C. Fusco and A. Fasolino, Velocity dependence of atomic-scale friction: A comparative study of the one- and two-dimensional Tomlinson model, *Phys. Rev. B* **71**, 045413 (2005).
- [29] L. Prandtl, Ein Gedankenmodell zur kinetischen Theorie der festen Körper, *ZAMM - J. Appl. Math. Mech.* **8**, 85 (1928).
- [30] G. A. Tomlinson, CVI. A molecular theory of friction, *Lond. Edinb. Dublin Philos. Mag. J. Sci.* **7**, 905 (1929).
- [31] H. Hölscher, U. D. Schwarz, and R. Wiesendanger, Modelling of the scan process in lateral force microscopy, *Surf. Sci.* **375**, 395 (1997).
- [32] P. Steiner, R. Roth, E. Gnecco, A. Baratoff, S. Maier, T. Glatzel, and E. Meyer, Two-dimensional simulation of superlubricity on NaCl and highly oriented pyrolytic graphite, *Phys. Rev. B* **79**, 045414 (2009).
- [33] O. E. Dagdeviren, Exploring load, velocity, and surface disorder dependence of friction with one-dimensional and two-dimensional models, *Nanotechnology* **29**, 315704 (2018).
- [34] O. E. Dagdeviren, Nanotribological properties of bulk metallic glasses, *Appl. Surf. Sci.* **458**, 344 (2018).
- [35] J. Israelachvili, *Intermolecular and Surface Forces* (Academic Press, London, 1991), 2nd ed.

- [36] N. W. Ashcroft and N. D. Mermin, *Solid State Physics* (Sounders College, Philadelphia, 1981).
- [37] P. M. Agrawal, B. M. Rice, and D. L. Thompson, Predicting trends in rate parameters for self-diffusion on FCC metal surfaces, *Surf. Sci.* **515**, 21 (2002).
- [38] M. Z. Baykara, O. E. Dagdeviren, T. C. Schwendemann, H. Mönig, E. I. Altman, and U. D. Schwarz, Probing three-dimensional surface force fields with atomic resolution: Measurement strategies, limitations, and artifact reduction, *Beilstein J. Nanotechnol.* **3**, 637 (2012).
- [39] Mathworks, *MATLAB Computing Environment and Programming Language* (Mathworks, Natick, MA, USA, 2017).
- [40] R. Wiesendanger, *Scanning Probe Microscopy and Spectroscopy: Methods and Applications* (Cambridge University Press, Cambridge, 1994).
- [41] O. E. Dagdeviren, J. Götzén, H. Hölscher, E. I. Altman, and U. D. Schwarz, Robust high-resolution imaging and quantitative force measurement with tuned-oscillator atomic force microscopy, *Nanotechnology* **27**, 065703 (2016).
- [42] B. Bhushan, J. N. Israelachvili, and U. Landman, Nanotribology: friction, wear and lubrication at the atomic scale, *Nature* **374**, 607 (1995).
- [43] J. B. Sokoloff, Theory of dynamical friction between idealized sliding surfaces, *Surf. Sci.* **144**, 267 (1984).
- [44] S. Y. Krylov and J. W. M. Frenken, The physics of atomic-scale friction: Basic considerations and open questions, *Phys. Status Solidi B* **251**, 711 (2014).
- [45] J. B. Sokoloff, Theory of the contribution to sliding friction from electronic excitations in the microbalance experiment, *Phys. Rev. B* **52**, 5318 (1995).
- [46] J. E. Sacco, J. B. Sokoloff, and A. Widom, Dynamical friction in sliding condensed-matter systems, *Phys. Rev. B* **20**, 5071 (1979).
- [47] V. L. Popov, Electronic contribution to sliding friction in normal and superconducting states, *J. Exp. Theor. Phys. Lett.* **69**, 558 (1999).
- [48] V. L. Popov, Electronic and phononic friction of solids at low temperatures, *Tribol. Int.* **34**, 277 (2001).
- [49] V. D. Georgii, Nanotribology: experimental facts and theoretical models, *Physics-Uspekhi* **43**, 541 (2000).
- [50] B. Gotsmann, Sliding on vacuum, *Nat. Mater.* **10**, 87 (2011).
- [51] A. I. Volokitin, B. N. J. Persson, and H. Ueba, Enhancement of noncontact friction between closely spaced bodies by two-dimensional systems, *Phys. Rev. B* **73**, 165423 (2006).
- [52] J. B. Sokoloff, Theory of energy dissipation in sliding crystal surfaces, *Phys. Rev. B* **42**, 760 (1990).
- [53] J. B. Sokoloff, Theory of atomic level sliding friction between ideal crystal interfaces, *J. Appl. Phys.* **72**, 1262 (1992).
- [54] V. L. Popov, Superslipperiness at Low Temperatures: Quantum Mechanical Aspects of Solid State Friction, *Phys. Rev. Lett.* **83**, 1632 (1999).
- [55] S. Kajita, H. Washizu, and T. Ohmori, Approach of semi-infinite dynamic lattice Green's function and energy dissipation due to phonons in solid friction between commensurate surfaces, *Phys. Rev. B* **82**, 115424 (2010).
- [56] L. Gross, F. Mohn, P. Liljeroth, J. Repp, F. J. Giessibl, and G. Meyer, Measuring the charge state of an adatom with noncontact atomic force microscopy, *Science* **324**, 1428 (2009).
- [57] F. J. Giessibl, High-speed force sensor for force microscopy and profilometry utilizing a quartz tuning fork, *Appl. Phys. Lett.* **73**, 3956 (1998).
- [58] G. H. Simon, M. Heyde, and H.-P. Rust, Recipes for cantilever parameter determination in dynamic force spectroscopy: Spring constant and amplitude, *Nanotechnology* **18**, 255503 (2007).
- [59] C. J. Chen, *Introduction to Scanning Tunneling Microscopy* (Oxford University Press, New York, 1993).
- [60] L. Gross, F. Mohn, N. Moll, B. Schuler, A. Criado, E. Guitián, D. Peña, A. Gourdon, and G. Meyer, Bond-order discrimination by atomic force microscopy, *Science* **337**, 1326 (2012).
- [61] B. J. Albers, T. C. Schwendemann, M. Z. Baykara, N. Pilet, M. Liebmann, E. I. Altman, and U. D. Schwarz, Three-dimensional imaging of short-range chemical forces with picometre resolution, *Nat. Nano* **4**, 307 (2009).
- [62] G. Langewisch, J. Falter, H. Fuchs, and A. Schirmeisen, Forces During the Controlled Displacement of Organic Molecules, *Phys. Rev. Lett.* **110**, 036101 (2013).
- [63] J. Tracey, F. Federici Canova, O. Keisanen, D. Z. Gao, P. Spijker, B. Reischl, and A. S. Foster, Flexible and modular virtual scanning probe microscope, *Comput. Phys. Commun.* **196**, 429 (2015).